Organic Geochemistry 150 (2020) 104123

Contents lists available at ScienceDirect

Organic Geochemistry

journal homepage: www.elsevier.com/locate/orggeochem

Algal biomarkers as a proxy for pCO_2: Constraints from late quaternary sapropels in the eastern Mediterranean

Caitlyn R. Witkowski [a,1,*], Marcel T.J. van der Meer [a], Brian Blais [b,c], Jaap S. Sinninghe Damsté [a,d], Stefan Schouten [a,d]

[a] Department of Marine Microbiology and Biogeochemistry, NIOZ Royal Netherlands Institute for Sea Research, and Utrecht University, 1790 AB Den Burg, Texel, the Netherlands
[b] Department of Science and Technology, Bryant University, Smithfield, RI 02917, USA
[c] Institute for Brain and Neural Systems, Brown University, Providence, RI 02912, USA
[d] Department of Geosciences, Utrecht University, 3508 TA Utrecht, the Netherlands

ARTICLE INFO

Article history:
Received 30 March 2020
Received in revised form 7 September 2020
Accepted 8 September 2020
Available online 15 September 2020

Keywords:
pCO_2
Organic geochemical proxies
Sapropels
Phytol
Alkenones

ABSTRACT

Records of carbon dioxide concentrations (partial pressure expressed as pCO_2) over Earth's history provide trends that are critical to understand our changing world. To better constrain pCO_2 estimations, here we test organic pCO_2 proxies against the direct measurements of pCO_2 recorded in ice cores. Based on the concept of stable carbon isotopic fractionation due to photosynthetic CO_2 fixation (ε_p), we use the stable carbon isotopic composition ($\delta^{13}C$) of the recently proposed biomarker phytol (from all photoautotrophs), as well as the conventionally used alkenone biomarkers (from specific species) for comparison, to reconstruct pCO_2 over several Quaternary sapropel formation periods (S1, S3, S4, and S5) in the eastern Mediterranean Sea. The reconstructed pCO_2 values are within error of the ice core values but consistently exceed the ice core values by ca. 100 μatm. This offset corresponds with atmospheric disequilibrium of present day $CO_{2[aq]}$ concentrations in the Mediterranean Sea from global pCO_2, equivalent to ca. 100 μatm, although pCO_2 estimates derived from individual horizons within each sapropel do not covary with the ice core values. This may possibly be due to greater variability in local $CO_{2[aq]}$ concentration changes in the Mediterranean, as compared with the global average pCO_2, or possibly due to biases in the proxy, such as variable growth rate or carbon-concentrating mechanisms. Thus, the offset is likely a combination of physiological or environmental factors. Nevertheless, our results demonstrate that alkenone- and phytol-based pCO_2 proxies yield statistically similar estimations (P-value = 0.02, Pearson's r-value = 0.56), and yield reasonable absolute estimations although with relatively large uncertainties (±100 μatm).

1. Introduction

The atmospheric partial pressure of CO_2 (pCO_2, expressed in μatm) has a significant impact on Earth system dynamics, including its climate-influencing role as a greenhouse gas. Assessing changes in pCO_2 over geological timescales may help us better understand current climate changes and predict the near future. Proxies, methods for quantitatively reconstructing past conditions, make it possible to look beyond the scope of direct measurements and provide secular trends in pCO_2 (Beerling and Royer, 2011). Although there are continual improvements of these pCO_2 proxies (Hollis et al., 2019), their accuracy remains largely uncertain and their incongruities increase with geologic time (Foster et al., 2017). Terrestrial proxies have been used to reconstruct pCO_2 over the past several hundred million years but often with unconstrained uncertainties, in part due to the limitations of the proxies and the effects of local carbon cycling that can occur in heterogenous terrestrial environments (e.g., Hollis et al., 2019). Marine proxies for pCO_2 reconstructions, on the other hand, tend to have more constrained homogenous signals and more continuous records but do not span as far back in time (Royer, 2013).

The marine-based pCO_2 proxy using the stable carbon isotopic fractionation associated with CO_2 fixation (ε_p) has been developed over the past several decades. ε_p relies on the kinetic isotope fractionation that occurs as algae capture CO_2 in their environment for photosynthesis, where the CO_2-fixing enzyme Rubisco more rapidly incorporates ^{12}C over ^{13}C into photoautotrophic biomass (Farquhar et al., 1982, 1989; Popp et al., 1989; Hayes et al.,

* Corresponding author at: Department of Marine Microbiology and Biogeochemistry, Royal Netherlands Institute for Sea Research, 1790AB Den Burg, the Netherlands.
E-mail address: caitlyn.witkowski@bristol.ac.uk (C.R. Witkowski).
[1] Current address: University of Bristol, School of Earth Sciences, Wills Memorial Building, Queens Road, Bristol BS8 1RJ, UK.

https://doi.org/10.1016/j.orggeochem.2020.104123
0146-6380/

1990). This fractionation results in a lower ^{13}C content ($\delta^{13}C$) of biomass than the inorganic carbon source that was fixed during photosynthesis. Increasing the availability of CO_2 has been shown to increase fractionation, and thus a positive relationship between pCO_2 and ε_p is generally observed (e.g., Popp et al., 1989; Jasper and Hayes, 1990; Freeman and Hayes, 1992).

Although sedimentary bulk organic matter can be used to reconstruct past $\delta^{13}C$ values of the algal biomass component (e.g., Hayes et al., 1999), species-specific algal biomarkers have been the primary target for decades (e.g., Jasper et al., 1994; Pagani, 2002). In the latter case, the $\delta^{13}C$ value of each biomarker is corrected for its offset from the $\delta^{13}C$ value of biomass (δ_p): δ_p is then used to reconstruct ε_p, together with the $\delta^{13}C$ value of dissolved CO_2 in the photic zone (δ_d) derived from e.g., planktic foraminiferal carbonate and corrected for the carbon isotopic fractionation of $CO_{2(aq)}$ with respect to HCO_3^-:

$$\varepsilon_p = 1000 \times [(\delta_d + 1000)/(\delta_p + 1000) - 1] \quad (1)$$

The relationship between $CO_{2[aq]}$ and ε_p is complex and several models have been applied. The most common and simplified equation is based on the theory first developed for higher plants (Farquhar et al., 1982, 1989) and subsequently modified for marine algae (Popp et al., 1989; Jasper and Hayes, 1990; Jasper et al., 1994; Bidigare et al., 1997):

$$pCO_2 = [b/(\varepsilon_f - \varepsilon_p)]/K_0 \quad (2)$$

In this equation, the apparent observed fractionation ε_p is subtracted from the maximum potential fractionation for CO_2 fixation (ε_f) and related to CO_2 via the catch-all term b, a term considering fractionation factors other than CO_2 such as growth rate, cell geometry, membrane permeability to CO_2, and the boundary layer thickness dependent on temperature, pH, and salinity (Rau et al., 1996; Laws et al., 1997; Popp et al., 1998; Bolton et al., 2016; Stoll et al., 2019). These combined parameters are equivalent to dissolved CO_2 conditions for the alga during its growth. Dissolved CO_2 may then be converted to atmospheric pCO_2 concentrations via the Henry's Law constant (K_0) using temperature and salinity (Weiss, 1974).

Most studies that reconstruct pCO_2 from ε_p have used long-chain alkenones (Jasper and Hayes, 1990; Pagani et al., 1999, 2005; Pagani, 2002; Zhang et al., 2013), biomarkers produced by a select group of haptophytes (Volkman et al., 1980). Due to the selectivity of the biomarkers, the difference between the $\delta^{13}C$ values of biomarker and biomass can be relatively well-constrained based on laboratory cultures of the specific alkenone-producing species (Riebesell et al., 2000). However, due to the fairly recent evolutionary history of alkenone producers, pCO_2 reconstructions are largely limited to last 45 Myr (Brassell, 2014). There are also some complicating factors with ε_p-based pCO_2 reconstructions, such as the evolutionary development of carbon concentrating mechanisms (CCMs) which actively pump bicarbonate in many marine phytoplankton (e.g., Laws et al., 1997), in contrast to the principal assumptions that ε_p is based on passive diffusion of $CO_{2[aq]}$ (e.g., Bidigare et al., 1997). The role and influence of CCMs has continued to be explored over the past two decades (Rost et al., 2003; Bach et al., 2013; Bolton et al., 2016). Although some studies suggest that CCMs are weakly expressed in haptophytes (e.g., Reinfelder, 2011), the most recent studies contrarily suggest that CCMs may limit the use of this proxy during periods of low pCO_2 (Badger et al., 2019; Stoll et al., 2019), i.e. when aqueous CO_2 concentrations fall below ca. 7 μmol L^{-1} (Badger, 2020). This proxy is further complicated by the nature of the catch-all term b which may vary over space and time (Zhang et al., 2019, 2020), making it difficult to constrain this parameter, and consequently pCO_2 reconstructions, over long timescales.

The ε_p-based pCO_2 proxy has recently been reevaluated for general phytoplankton biomarkers, compounds derived from a multitude of marine algal species (Witkowski et al., 2018, 2019, 2020). There has been minimal proxy development research on ε_p from general algal biomarkers, with the exception of some paleo-pCO_2 applications of chlorophyll *a* products, including its porphyrin core (Popp et al., 1989; Freeman and Hayes, 1992) and the diagenetic product of its phytol side-chain phytane (Bice et al., 2006; Sinninghe Damsté et al., 2008; van Bentum et al., 2012; Naafs et al., 2016), which should have the same $\delta^{13}C$ value as phytol given that there are no additions or loss of C during diagenetic transformation. Because chlorophyll *a* is the vital light harvesting pigment in all photoautotrophs, it includes eukaryotic algae, cyanobacteria, and plants in both marine and terrestrial environments, offering greater spatial and temporal ubiquity throughout the geologic record as compared with its species-specific counterparts, i.e. alkenones limited to ca. 45 Ma (Brassell, 2014). At the same time, chlorophyll *a* and its products offer more specificity than bulk organic matter; bulk organic matter raises concerns of isotopic heterogeneity with different organisms contributing different types of preserved organic matter e.g., carbohydrates, proteins, and lipids, each with distinct $\delta^{13}C$ values (Hayes, 1993) and distinct diagenetic changes to those $\delta^{13}C$ values e.g., via carbohydrate sulfurization (Sinninghe Damsté et al., 1998). Given that chlorophyll *a* rapidly breaks down and is not prone to lateral transport, phytol and its diagenetic products are likely deposited and buried close to their source organism. In our recent reevaluation of phytane over the Phanerozoic, we thus focused our efforts on open marine settings with minimal terrestrial input in order to limit the source of organisms to primarily algae (Witkowski et al., 2018). Phytane shows similar estimates to other pCO_2 proxies over the Phanerozoic and offers the longest marine-based pCO_2 record currently available (Witkowski et al., 2018). However, although some modern studies across naturally occurring high CO_2 gradients have recently been conducted (Witkowski et al., 2019, 2020), the accuracy of this proxy has not been tested on shorter geologic timescales with smaller variability in pCO_2 nor compared with the more commonly applied alkenone-based pCO_2 proxy.

Here, we test this method in late Pleistocene to Holocene organic matter-rich marls from the Mediterranean Sea known as sapropels (S1, S3, S4, and S5) so that ε_p-based pCO_2 proxy values derived from a general algal biomarker can be compared with directly measurable pCO_2 values, i.e. trapped air bubbles in ice, over both the glacial-inception and the interglacial period that shows some pCO_2 fluctuations, albeit relatively small (< 50 μatm). This comparison allows us to evaluate the use of these general algal biomarkers as ε_p-based proxies for pCO_2 in deep-time. Finally, we compare this approach to ε_p values from alkenones, a more commonly applied method for pCO_2 reconstructions.

2. Materials and methods

A 920.5 cm long piston core (containing sapropels S3, S4, and S5) and accompanying multi-core (containing sapropel S1) were collected in the southeast Levantine Sea during the January 2016 R/V *Pelagia* research cruise 64PE406 at Station 1 (33°18.14898′ N, 33°23.71998′ E). Sapropels and their preservation were assessed using Ti, Mn, Br, and Ba intensities derived from X-Ray fluorescence core-scanning. The age model of the cores was derived by comparison of the Ba profile to sapropel boundaries (Grant et al., 2016), which have been linked to the ages of the well-dated Soreq cave record (Bar-Matthews et al., 2003). All samples were taken in 1 cm width horizons, all within the visually defined dark organic-rich sapropel layer, and the horizons used for organic geochemistry

were taken approximately every 3 cm. Several individual horizons were taken from each sapropel (two layers sampled within S1, three layers in S3, four layers within S4, and eight layers within S5).

Sediments were freeze-dried and homogenized using a mortar and pestle. For sapropels S1, S3, and S4, lipids were extracted with a Dionex 250 accelerated solvent extractor at 100 °C, 7.6×10^6 Pa using dichloromethane (DCM): methanol (MeOH; 9:1, v/v). For the sapropel S5, lipids were previously extracted using Bligh-Dyer extraction using MeOH:DCM:phosphate buffer (2:1:0.8, v/v/v) (Bale et al., 2019). All extracts were refluxed for 1 h with 1 N of KOH in MeOH to hydrolyze the lipids and then neutralized to pH 5 with 2 N HCl in MeOH. Bi-distilled water (2 ml) and DCM (2 ml) were added (5×) to the hydrolyzed centrifuge tubes and the DCM layers, containing the extractable compounds, were pooled, and then dried over Na_2SO_4. They were then eluted over an Al_2O_3 column into apolar (hexane:DCM, 9:1, v/v), ketone (DCM), and polar (DCM:MeOH, 1:1, v/v) fractions, respectively. The polar fractions were silylated with pyridine: N,O-bis(trimethyl silyl)trifluoroacetamide (BSTFA) (1:1, v/v) and heated for 1 h at 60 °C.

Silylated polar fractions and ketone fractions were analyzed on an Agilent 7890B gas chromatograph with flame ionization detector (GC-FID), an Agilent 5975C VL MSD gas chromatograph–mass spectrometer (GC–MS), and Isolink II gas chromatograph–isotope ratio mass spectrometer (GC–irMS). On the GC-FID, ketone fractions were run on a CP-Sil 5 column (50 m × 0.32 mm; d_f 0.12 μm) with a starting oven temperature of 70 °C ramped to 200 °C at 20 °C/min and then to 320 °C at 3 °C/min for 25 min. The silylated polar fractions were run on a CP-Sil 5 column (25 m × 0.32 mm; d_f 0.12 μm) with a starting oven temperature of 70 °C ramped to 130 °C at 20 °C/min and then to 320 °C at 4 °C/min for 10 min. Both fractions were run on GC–MS and irMS using the same column and oven ramp program as the GC-FID method used for the polar fractions. An in-house GC standard mix of *n*-alkanes and fatty acids were used for all three instruments to check GC performance. The performance of the GC–irMS was tested using additional standards of completely deuterated (99.1%) C_{20} (−32.7‰) and C_{24} (−27.0‰), which were co-injected with the daily GC standard, as well as each sample, to check reproducibility of the carbon isotope values (within 0.5‰). The GC–irMS Isolink II combustion reactor was daily oxidized for 15 min, He backflushed for 10 min, and purged for 5 min. Every analysis ended with a 2 min post-sample seed oxidation and, in addition, 1 h oxidation sequences were run once week. All samples were run in at least duplicate. Silylated phytol was corrected for the three additional C atoms in the trimethylsilyl group by using the predetermined $\delta^{13}C$ value of BSTFA (−32.2‰).

The $\delta^{13}C$ value of carbonate in the surface-dwelling planktic foraminifera *Globigerinoides ruber* was measured at 1 cm resolution over the same core as the organic compounds. Sampling methods are specified in Geerken (2019). Stable isotopes of 15–45 μg carbonate crushed from *G. ruber* shells were analyzed using a Kiel-IV device coupled to a Thermo-Finnigan MAT253. Standards were run every several samples, using in-house standards (NFHS-1, $\delta^{13}C = 0.854$‰) and international carbonate standards (NBS-19, $\delta^{13}C = 1.95$‰). The mean external reproducibility was less than ± 0.05‰.

3. Results and discussion

3.1. Estimating pCO_2 from the $\delta^{13}C$ values of phytol and alkenones

Several studies on eastern Mediterranean sapropel organic matter have shown a dominant input of mainly marine algal biomarkers, in particular the long-chain unsaturated ketones, alkanediols, loliolide, and sterols (ten Haven et al., 1987b, 1987a; Bouloubassi et al., 1999), supporting a phytoplankton origin for phytol. Indeed, we observe similar biomarkers in our sediments and minimal terrestrial input (e.g., odd-over-even long-chain *n*-alkanes and triterpenoids). The precise contributions of different species to the phytoplankton pool are difficult to define, but evidence of calcareous nannoplankton, diatoms, and dinoflagellate cysts are common during sapropel periods (e.g., Giunta et al., 2006).

Multiple 1 cm horizons from each sapropel (S1, S3, S4, and S5) yielded enough material for carbon isotope analysis of phytol and alkenones. The $\delta^{13}C$ values of phytol ranged from −22.3‰ to −27.7‰ throughout the whole section (Table 1). The $\delta^{13}C$ values of phytol varied in each individual sapropel: S1 from −26.4‰ to −26.9‰, S3 from −22.3‰ to −24.5‰, S4 from −22.9‰ to −27.7‰, and S5 from −23.5‰ to −25.0‰ (Table 1). The $C_{37:3}$, $C_{37:2}$, $C_{38:3}$, and $C_{38:2}$ alkenones were detected in the sapropels. We report the integrated isotopic composition value of $C_{37:3}$ and $C_{37:2}$ alkenones, ranging from −24.5‰ to −27.0‰ over the whole section (Table 1), a smaller range than observed for phytol. The $\delta^{13}C$ values of alkenones ranged within sapropel S1 from −25.5‰ to −25.9‰, S3 from −24.5‰ to −25.1‰, S4 at −25.2‰ to −27.0‰, and S5 from −24.8‰ to −26.2‰ (Table 1). The larger range in $\delta^{13}C$ values of phytol is mainly due to the much larger variability observed in sapropel S4 compared to the other sapropels; although not as extreme, there is also a larger range of values in S4 for the $\delta^{13}C$ values of alkenones. The reason for this larger variability in S4 is unclear and will be later discussed.

ε_p was calculated from the $\delta^{13}C$ value of organic matter (δ_p) and the $\delta^{13}C$ value of dissolved CO_2 in the photic zone (δ_d) using Eq. (1). δ_p was calculated from the $\delta^{13}C$ value of each biomarker corrected for its offset from the $\delta^{13}C$ value of biomass. For phytol we used an average offset of 3.5 ± 1.3‰ s.d. based on 23 laboratory cultures and modern environmental studies using a variety of algal and cyanobacterial species (Sakata et al., 1997; Schouten et al., 1998; Riebesell et al., 2000; van Dongen et al., 2002; Oakes et al., 2005; Wilkes et al., 2017), and for alkenones we used an average offset of 4.2 ± 0.9‰ s.d. based on the average of five laboratory cultures of *E. huxleyi* (Jasper and Hayes, 1990; Schouten et al., 1998; Riebesell et al., 2000; Laws et al., 2001; van Dongen et al., 2002), with many of these studies conducted under the same conditions for both phytol and alkenones, and some even from the same organism. The δ_d is derived from the high-resolution record of $\delta^{13}C$ values of the surface-dwelling planktic foraminifera *Globigerinoides ruber* from the same core (Supplementary Tables S1 and S2). δ_d was then corrected for temperature-dependent carbon isotopic fractionation of dissolved CO_2 with respect to HCO_3^- using the equation from Mook et al. (1974) and Weiss (1974):

$$\delta_d = \delta^{13}C_{carbonate} - 1 + (24.12 - 9866/T) \quad (3)$$

For temperature (expressed in K), we calculated sea surface temperature (SST) from $U^{K'}_{37}$ based on the alkenones reported here and using the global core top calibration (Müller et al., 1998). The $U^{K'}_{37}$-based SSTs ranged from 17.7 °C to 23.5 °C (Table 1), in agreement with those previously reported for sapropels (Emeis et al., 2003).

ε_p values derived from phytol ranges from 9.0‰ to 15.0‰ over all sapropels, ranging from 13.4‰ to 13.7‰ in S1, 9.0‰ to 11.5‰ in S3, 10.5‰ to 15.0‰ in S4, and 9.8‰ to 11.1‰ in S5 (Table 1). ε_p values derived from alkenones ranges from 10.4‰ to 13.2‰ over all sapropels, ranging from 11.3‰ to 12.4‰ in S1, 10.9‰ to 11.3‰ in S3, 12.2‰ to 13.2‰ in S4, and 10.4‰ to 11.6‰ in S5 (Table 1). The amalgamation of error propagation was calculated using Monte Carlo simulations in which each individual parameter with its associated uncertainty was included, as described by Witkowski

Table 1
Sapropels (S) with individual horizons marked by core (MC = multicore, PC = piston core) and depth over the past 130 thousand years (ka). Concentrations of $C_{37:2}$ and $C_{37:3}$ alkenones, $U^{K'}_{37}$ index and associated sea surface temperature (SST) estimates, and the $\delta^{13}C$ values, calculated ε_p, and estimated pCO_2 derived from alkenones (C_{37}) and phytol (Ph) with associated uncertainties calculated with Monte Carlo simulations, shown in standard deviation (s.d.). pCO_2 estimations do not have uniform negative (–) and positive (+) standard deviation and are thus both shown.

S	ka	Core–Depth	$C_{37:2}$	$C_{37:3}$	$U^{K'}_{37}$	SST	$\delta^{13}C_{C37}$	s.d.	$\delta^{13}C_{Ph}$	s.d.	$\varepsilon_{p\ C37}$	s.d.	$\varepsilon_{p\ Ph}$	s.d.	$pCO_{2\ C37}$	–	+	$pCO_{2\ Ph}$	–	+
1	9.4	MC 32	88	34	0.72	20.5	–25.9	0.5	–26.4	0.5	12.5	0.6	13.7	0.8	373	115	122	411	108	116
1	10.2	PC 10 1–2	689	309	0.69	19.6	–25.5	0.5	–26.9	0.5	11.3	0.6	13.4	0.8	335	102	109	392	103	109
3	83.1	PC 8 66–67	267	144	0.65	18.4	–25.1	0.5	–24.5	0.5	11.4	0.6	11.5	0.8	327	100	107	330	87	91
3	84.2	PC 8 68–69	225	93	0.71	20.1	–24.8	0.5	–22.3	0.5	10.9	0.6	9.1	0.8	333	102	108	297	77	80
3	85.3	PC 8 71–72	374	133	0.74	21.0	–24.5	0.5	–22.4	0.5	10.9	0.6	9.5	0.8	341	104	111	312	81	86
4	106.6	PC 7 52–53	783	344	0.70	19.7	–26.6	0.5	–27.6	0.5	13.2	0.6	15.0	0.8	388	119	127	448	117	126
4	107.1	PC 7 54–55	461	274	0.63	17.7	–27.0	0.5	–25.0	0.5	12.8	0.6	11.5	0.8	355	111	117	324	87	93
4	107.3	PC 7 55–56	70	16	0.81	23.2	–25.2	0.5	–22.9	0.5	12.2	0.6	10.5	0.8	393	121	128	353	89	94
4	107.8	PC 7 56–57	314	144	0.69	19.5	–26.5	0.5	–27.7	0.5	12.3	0.6	14.2	0.8	359	110	117	416	117	127
5	121.6	PC 6 17–18	80	19	0.81	23.2	–25.1	0.5	–23.8	0.5	10.5	0.6	10.0	0.8	352	108	113	340	88	93
5	122.2	PC 6 20–21	287	68	0.81	23.2	–25.2	0.5	–23.9	0.5	10.7	0.6	10.1	0.8	357	108	116	344	90	95
5	122.5	PC 6 21–22	324	74	0.81	23.4	–24.8	0.5	–24.1	0.5	10.4	0.6	10.4	0.8	353	108	113	352	91	97
5	122.6	PC 6 22–23	133	30	0.82	23.5	–25.3	0.5	–23.5	0.5	10.9	0.6	9.8	0.8	364	113	116	339	89	93
5	124.0	PC 6 28–29	1225	458	0.73	20.7	–25.5	0.5	–24.0	0.5	11.0	0.6	10.2	0.8	341	104	110	323	85	88
5	125.1	PC 6 33–34	531	176	0.75	21.4	–26.2	0.5	–25.0	0.5	11.6	0.6	11.1	0.8	361	111	118	350	93	99
5	125.8	PC 6 36–37	2011	759	0.73	20.7	–25.9	0.5	–24.7	0.5	11.6	0.6	11.0	0.8	353	108	115	341	89	94
5	127.4	PC 6 43–44	242	65	0.79	22.6	–25.5	0.5	–24.4	0.5	11.3	0.6	10.9	0.8	364	112	118	355	93	98

et al. (2018), and expressed as 1 s.d. (68%; Supplementary Tables S1 and S2). Parameter uncertainties included the $\delta^{13}C$ value of the biomarkers (0.5‰), the $\delta^{13}C$ value of the carbonates (0.1‰), SST (2 °C), and the offset between the $\delta^{13}C$ value of biomass from each biomarker (1.3‰ for phytol; 0.9‰ for alkenones), culminating to an uncertainty in ε_p values of ca. ± 1.4‰ for both phytol and alkenones. When compared within the same sediments and thus time periods, there is a striking similarity between these two proxies (Fig. 1).

Individual ε_p values calculated from the $\delta^{13}C$ value of phytol (derived from the whole phytoplankton community) and those calculated from the $\delta^{13}C$ value of alkenones (derived from species-specific producers) yield statistically similar values (*P*-value = 0.005, Pearson's *r*-value = 0.645). This suggests that isotopic fractionation is similar between haptophyte algae and other phytoplankton, or possibly that they represent a similar source, i.e. that haptophyte algae dominate the overall phytoplankton pool. There are several data points which lay just outside the one-to-one line between ε_p values derived from alkenones vs phytol, all from the onset of sapropels S1 and S4. At the onset, changes in sea surface salinity and nutrient input associated with a large freshwater input from the African continent, including the Nile (Lourens et al., 1996; Rohling and De Rijk, 1999), likely influenced the overall phytoplankton community, in which the phytol-producing species (the overall photoautotrophic community) may have differed from alkenone-producing species in average cell size or growth rates.

To reconstruct pCO_2 from ε_p, Eq. (2) was used. A *b* value of 170 ± 43‰ kg μM^{-1} has been used for phytol based on a compilation of 18 studies of the $\delta^{13}C$ values of modern surface sediment organic matter (see Witkowski et al., 2018), as well as values of 170‰ kg μM^{-1} applied in previous studies that have estimated pCO_2 from phytol's diagenetic product phytane (Bice et al., 2006; Sinninghe Damsté et al., 2008; van Bentum et al., 2012; Naafs et al., 2016; Witkowski et al., 2018). For C_{37} alkenones, the value for *b* in modern oceans has been shown to range from ca. 55 to 400 with an average of 165 ± 53‰ kg μM^{-1} based on a compilation of modern alkenone-based environmental studies (Pagani, 2013). Given the similar values and large uncertainties in *b* values for both phytol and C_{37} alkenones, here we use *b* = 170 ± 50‰ kg μM^{-1} for both. For ε_f, we use an average of 26.5‰ (±1.5‰ uniform uncertainty) for both phytol and alkenones to reflect the ε_f of 25–28‰ observed for laboratory cultures for a multitude of algal and cyanobacterial species (Goericke et al., 1994). Finally, K_0 is calculated from temperature and salinity (Weiss, 1974), in which SST is derived from the alkenone-based $U^{K'}_{37}$ temperature proxy measured in the same sapropel layer (Table 1), while sea surface salinity (SSS) is based on the average Mediterranean values for this region, i.e. ca. 39 ppt (van der Meer et al., 2007), although decreased values for SSS as low as 33 ppt during the onset of sapropel deposition have been reported (van der Meer et al., 2007). Overall, the impact of this salinity change on the final pCO_2 estimate is relatively minimal to moderate, ranging between 1 and 53 μatm.

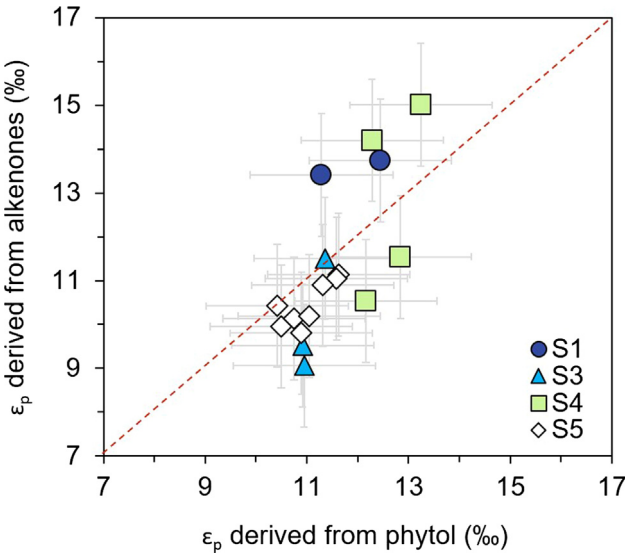

Fig. 1. ε_p calculated from the $\delta^{13}C$ of phytol and alkenones over four sapropels: S1 (purple circles), S3 (blue triangles), S4 (green squares), and S5 (white diamonds). Orange dashed line illustrates a 1:1 line. (For interpretation of the references to colour in this figure legend, the reader is referred to the web version of this article.)

The resulting estimates for pCO_2 look similar for the two biomarkers, ranging from ca. 300 μatm to 450 μatm for phytol and from ca. 330 μatm to 390 μatm for alkenones for all sapropel time intervals (Fig. 2; Supplementary Tables S1 and S2). Uncertainties in the estimates were calculated from Monte Carlo simulations, which consider the sum effect of each individual parameter on the final estimations for pCO_2 as described above. For individual sapropels (Fig. 2), phytol-based pCO_2 estimates in S1 range from ca. 390 μatm to 415 μatm with uncertainty estimations of ca. –90/

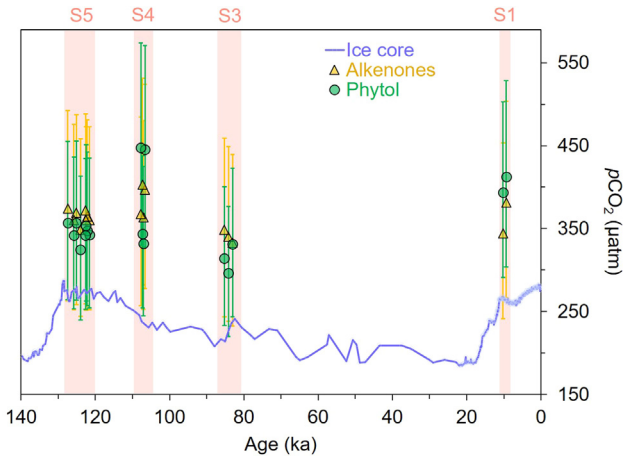

Fig. 2. pCO_2 estimated from the $\delta^{13}C$ of phytol (green circles) and alkenones (golden triangles), including standard deviations determined by Monte Carlo simulations that the culmination of all individual parameter uncertainties. Red bands highlight the four sapropels deposited over the past 140 ka. Purple line shows direct pCO_2 measurements from gas bubbles trapped in ice cores (Petit et al., 1999; Monnin et al., 2001; Pepin et al., 2001). (For interpretation of the references to colour in this figure legend, the reader is referred to the web version of this article.)

+105 µatm, S3 from ca. 300 µatm to 330 µatm (ca. –65/+75 µatm s.d.), S4 from ca. 325 µatm to 450 µatm (uncertainty ca. –85/+100 µatm s.d.), and S5 from 325 µatm to 355 µatm (uncertainty ca. –70/+80 µatm s.d.). Alkenone-based pCO_2 estimates in S1 range from ca. 340 µatm to 375 µatm (ca. –75/+85 µatm s.d.), S3 from ca. 330 µatm to 345 µatm (ca. –70/+80 µatm s.d.), S4 from ca. 355 µatm to 395 µatm (ca. –80/+95 µatm s.d.), and S5 from 345 µatm to 370 µatm (ca. –75/+85 µatm s.d.). When correlating individual data points at the same ages over the course of the record, phytol- and alkenone-based pCO_2 estimations are statistically similar (*P*-value = 0.020, Pearson's *r*-value = 0.559), and with similar uncertainties (±100 µatm), suggesting that these two biomarkers yield comparable estimates of past pCO_2.

3.2. Comparison of reconstructed pCO_2 with ice core data

Past global atmospheric pCO_2 recorded in ice core gas bubbles (Petit et al., 1999; Pépin et al., 2001) have values in glacial-inception pCO_2 of 226 µatm at ca. 84 ka (same timing as S3) and 234 µatm at ca. 107 ka (same timing as S4) and have values in the interglacial period of pCO_2 of 265 µatm at ca. 10 ka (same timing as S1) and 271 µatm at ca. 124 ka (same timing as S5). Our individual proxy estimations are just within error of this ice core data (Fig. 2). However, individual pCO_2 estimations based on alkenone- and phytol-derived ε_p do not covary with the individual ice core pCO_2 data (for phytol: *P*-value = 0.780, Pearson's *r*-value = 0.073; for alkenones: *P*-value = 0.784, Pearson's *r*-value = 0.072). The lack of correlation of the individual data between our reconstructed Mediterranean Sea values with that of the ice core can be explained either from the mechanics of the proxy, such as the physiological factor *b* or CCMs, or from local oceanographic variability.

Firstly, potential issues may arise from the mechanics of the proxy itself, such as the catch-all physiological parameter *b* and/or CCMs. The *b* value is based on parameter-by-parameter uncertainty analysis which uses the global average of 170 ± 50‰ kg μM^{-1} for all phytoplankton, a reasonable approach in paleoreconstructions when there is a lack of data for the accurate estimation of *b*, but nonetheless making this an intrinsically difficult parameter to constrain. During the unusual sapropel-forming events, *b* could be influenced by increased productivity, a possible result of freshwater input from the Nile River coupled with enhanced upward advection of nutrients to the base of the photic zone, fueling a productive deep chlorophyll maximum or a starved surface layer (Grelaud et al., 2012). As the *b* factor has been shown to be a mutable variable (Zhang et al., 2019), any major changes to the *b* value during sapropel deposition or among the four different sapropels may explain the lack of correlation with the ice core data.

CCMs in phytoplankton could also affect the mechanisms of the proxy, especially given that this is a period of low pCO_2. In order to supplement CO_2 under insufficient levels of pCO_2, many phytoplankton have been shown to have developed CCMs which actively pump HCO_3^- at the active site of Rubisco (e.g., Raven and Beardall, 2014; Kottmeier et al., 2016). This differs from the diffusive model used here (Eqs. (1) and (2)), which is based on the assumption that dissolved $CO_{2[aq]}$ (only) passively enters the algal cell, a concept observed in laboratory cultures where CO_2 availability is high relative to cellular carbon demand (Francois et al., 1993; Rau et al., 1996). Active uptake is a concern given the substantial $\delta^{13}C$ difference between bicarbonate (0‰) and CO_2 (–8‰) (Mook et al., 1974) and because they can decouple the amount of intracellular CO_2 from outside the cell. Results of a statistical multilinear regression model, that quantitatively considers factors influencing ε_p values in cultures of alkenone-producing algae, suggests that there is lower sensitivity of ε_p to pCO_2 than proposed by the diffusive model (Stoll et al., 2019). CCMs have been invoked to explain the muted response of pCO_2 reconstructed from the $\delta^{13}C$ values of alkenones as compared with ice core pCO_2 data, as well as pCO_2 reconstructed from the $\delta^{11}B$ of foraminifer shells (Badger et al., 2019) when aqueous carbon dioxide concentrations fall below 7 $\mu molL^{-1}$ (Badger, 2020). Finally, it has been proposed that stable carbon isotopic fractionation is impacted by a rate-limiting step upstream of Rubisco under excess photon flux, rather than fractionation of Rubisco, thus changing the sensitivity of fractionation to CO_2 changes (Wilkes and Pearson, 2019).

Apart from issues that may arise from the proxy itself, local variability may be a possible explanation for this difference between the individual proxy estimates and the individual ice core data. In other words, the proxies may reflect changes in their local environment. Dissolved CO_2 concentrations are more likely to vary locally over time, especially in a semi-enclosed Mediterranean Sea, as compared with the more homogeneous atmospheric pCO_2. This perhaps explains the high variability within S4 (Fig. 2), where the standard deviation for the individual pCO_2 estimations are ca. 57 µatm. When these S4 data are removed from the overall dataset, a notably improved correlation between the biomarker pCO_2 reconstructions with the ice core data can be seen (phytol: *P*-value = 0.075, Pearson's *r*-value = 0.509; alkenones: *P*-value = 0.028, Pearson's *r*-value = 0.606). These local offsets may be caused by the many influences on $CO_{2[aq]}$ in the Mediterranean Sea, such as the cyclic influence of freshwater input from the Nile that may change alkalinity, temperature, nutrient availability, and other seawater components. Local changes could affect the $\delta^{13}C$ values of the CO_2 via periodic deep-water convection (Melki et al., 2010), causing the mixing of ^{13}C-depleted CO_2 from below the chemocline in the otherwise-stratified Mediterranean water column during sapropel formation (Küspert, 1982). This effect on the $\delta^{13}C$ values of CO_2 used by phytoplankton is, however, not observed in the planktic foraminifera signal as it remains fairly constant (Supplementary Tables S1 and S2).

With these possible issues in mind, there is likely some combination of factors to explain why individual data points differ between the ice core data and the estimated organic proxy calculations. When data of the individual layers are combined per sapropel to obtain a clear view on general trends, a consistent offset of the ε_p-based pCO_2 estimations and the pCO_2 from ice core data by ca. 100 µatm is observed for all sapropels (Fig. 2). This offset

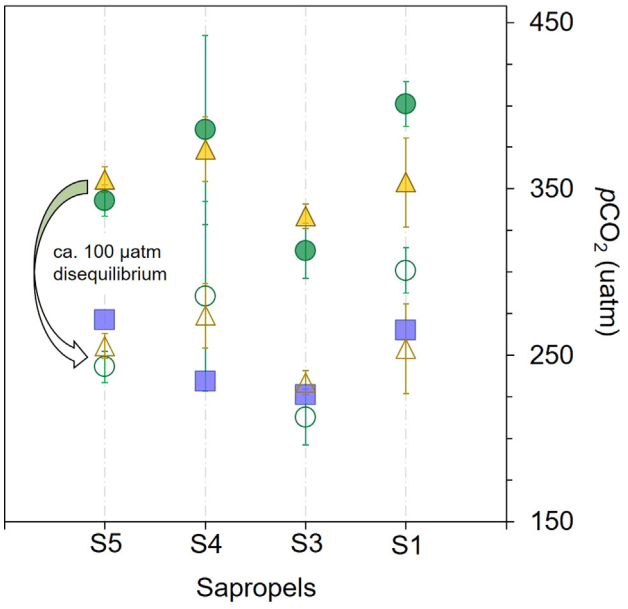

Fig. 3. Averages for pCO_2 estimates for the time period of each individual sapropel from phytol (circles) and alkenones (triangles), showing both estimates based on the described parameters (filled) and the values corrected for a 100 µatm offset that accounts for the disequilibrium of the Mediterranean Sea with atmospheric pCO_2 (Bégovic and Copin-Montégut, 2002). Standard deviations are determined by Monte Carlo simulations that culminate all individual parameter uncertainties. Averages for direct pCO_2 measurements from gas bubbles trapped in ice cores (purple squares; Petit et al., 1999; Monnin et al., 2001; Pepin et al., 2001). (For interpretation of the references to colour in this figure legend, the reader is referred to the web version of this article.)

may be due to the disequilibrium of the Mediterranean Sea with atmospheric pCO_2 due to the relatively high alkalinity in the Mediterranean Sea (Rivaro et al., 2010), which has been observed to have the equivalent $CO_{2[aq]}$ of ca. 100 µatm above the global average of pCO_2 (Bégovic and Copin-Montégut, 2002). Assuming that this disequilibrium also holds for times of sapropel deposition, the average values for the ε_p-based pCO_2 corrected for this offset are quite similar compared to the ice core pCO_2 values (Figs. 2 and 3), except for sapropel S4 which, as discussed above, behaves differently compared to other sapropels. Hence, if this offset is taken into consideration, both phytol and alkenone proxies based on ε_p seem to yield reasonable pCO_2 estimations in the late Pleistocene to Holocene.

4. Conclusions

The $\delta^{13}C$ values of a potential biomarker for pCO_2, phytol, as well as the $\delta^{13}C$ values of its established biomarker counterpart, alkenones, were used to calculate photosynthetic isotopic fractionation (ε_p) and estimate pCO_2 from Quaternary Mediterranean Sea sapropels. Phytol- and alkenone-based pCO_2 values yielded similar estimations, i.e. 300 µatm to 450 µatm for phytol and ca. 330 µatm to 390 µatm for alkenones. These values overestimate global atmospheric pCO_2 by ca. 100 µatm, which corresponds with the enhanced dissolved CO_2 concentrations in the Mediterranean Sea due to its high alkalinity. Given this disequilibrium consideration, the ε_p proxy for reconstructing pCO_2 seems to reflect CO_2 concentrations during Quaternary sapropel formation in the Mediterranean. Although these results are favorable, there is a lack of correlation between changes in the individual reconstructed pCO_2 values from the two biomarkers and individual pCO_2 values from ice core data, most notably in S4. Importantly, the ranges for the phytol- and alkenone-based pCO_2 estimates are much larger than that observed in the ice core pCO_2 values, which largely explains this lack of covariation. This larger variability in range for the proxies may be due to higher local variability in the semi-enclosed Mediterranean, e.g., influencing dissolved CO_2 and the *b* factor, as well as potential influences from carbon concentrating mechanisms. This variability may suggest that open marine settings with more homogenized and stable conditions are more suitable for ε_p-based pCO_2 reconstructions. Nevertheless, our results show that ε_p-based pCO_2 estimates derived from general algal biomarkers may be as useful as those of alkenones and provide reasonable estimates.

Declaration of Competing Interest

The authors declare that they have no known competing financial interests or personal relationships that could have appeared to influence the work reported in this paper.

Acknowledgements

We thank Esmee Geerken, Lynn Kruithof, and Gert-Jan Reichart for the use of the $\delta^{13}C$ values of carbonate derived from the planktonic foraminifera *G. ruber*, Rick Hennekam for his help in sampling the core and commenting on an early draft of this manuscript, and Jort Ossebaar and Ronald van Bommel at the NIOZ for technical support, as well everyone involved in the R/V *Pelagia* research cruise 64PE406 funded by the Netherlands Earth System Science Center (NESSC). We thank two anonymous reviewers, Associate Editor Andy Revill, and Co-Editor in Chief John Volkman for their comments which improved the manuscript. This project was funded through a NESSC gravitation grant (024.002.001) to JSSD and SS from the Dutch Ministry for Education, Culture and Science, The Netherlands.

Appendix A. Supplementary material

Supplementary data to this article can be found online at https://doi.org/10.1016/j.orggeochem.2020.104123.

Associate Editor–**Andy Revill**

References

Bach, L.T., MacKinder, L.C.M., Schulz, K.G., Wheeler, G., Schroeder, D.C., Brownlee, C., Riebesell, U., 2013. Dissecting the impact of CO_2 and pH on the mechanisms of photosynthesis and calcification in the coccolithophore *Emiliania huxleyi*. New Phytologist 199, 121–134.

Badger, M.P.S., 2020. Alkenone isotopes show evidence of active carbon concentrating mechanisms in coccolithophores as aqueous carbon dioxide concentrations fall below 7 $\mu molL^{-1}$. EarthArXiv Preprints. https://doi.org/10.31223/osf.io/3ywqd.

Badger, M.P.S., Chalk, T.B., Foster, G.L., Bown, P.R., Gibbs, S.J., Sexton, P.F., Schmidt, D. N., Pälike, H., Mackensen, A., Pancost, R.D., 2019. Insensitivity of alkenone carbon isotopes to atmospheric CO_2 at low to moderate CO_2 levels. Climate of the Past 15, 539–554.

Bale, N.J., Hennekam, R., Hopmans, E.C., Dorhout, D., Reichart, G.J., van der Meer, M., Villareal, T.A., Sinninghe Damsté, J.S., Schouten, S., 2019. Biomarker evidence for nitrogen-fixing cyanobacterial blooms in a brackish surface layer in the Nile River plume during sapropel deposition. Geology 47, 1088–1092.

Bar-Matthews, M., Ayalon, A., Gilmour, M., Matthews, A., Hawkesworth, C.J., 2003. Sea-land oxygen isotopic relationships from planktonic foraminifera and speleothems in the Eastern Mediterranean region and their implication for paleorainfall during interglacial intervals. Geochimica et Cosmochimica Acta 67, 3181–3199.

Beerling, D.J., Royer, D.L., 2011. Convergent cenozoic CO_2 history. Nature Geoscience 4, 418–420.

Bégovic, M., Copin-Montégut, C., 2002. Processes controlling annual variations in the partial pressure of CO_2 in surface waters of the central northwestern Mediterranean Sea (Dyfamed site). Deep-Sea Research Part II: Topical Studies in Oceanography 49, 2031–2047.

Bice, K.L., Birgel, D., Meyers, P.A., Dahl, K.A., Hinrichs, K.U., Norris, R.D., 2006. A multiple proxy and model study of Cretaceous upper ocean temperatures and

atmospheric CO_2 concentrations. Paleoceanography 21, PA2002. https://doi.org/10.1029/2005PA001203.
Bidigare, R.R., Fluegge, A., Freeman, K.H., Hanson, K.L., Hayes, J.M., Hollander, D., Jasper, J.P., King, L.L., Laws, E.A., Milder, J., Millero, F.J., Pancost, R., Popp, B.N., Steinberg, P.A., Wakeham, S.G., 1997. Consistent fractionation of ^{13}C in nature and in the laboratory: Growth-rate effects in some haptophyte algae. Global Biogeochemical Cycles 11, 279–292.
Bolton, C.T., Hernández-Sánchez, M.T., Fuertes, M.Á., González-Lemos, S., Abrevaya, L., Mendez-Vicente, A., Flores, J.A., Probert, I., Giosan, L., Johnson, J., Stoll, H.M., 2016. Decrease in coccolithophore calcification and CO_2 since the middle Miocene. Nature Communications 7, 10284. https://doi.org/10.1038/ncomms10284.
Bouloubassi, I., Rullkötter, J., Meyers, P.A., 1999. Origin and transformation of organic matter in Pliocene-Pleistocene Mediterranean sapropels: Organic geochemical evidence reviewed. Marine Geology 153, 177–197.
Brassell, S.C., 2014. Climatic influences on the Paleogene evolution of alkenones. Paleoceanography 29, 255–272.
Emeis, K.-C., Schulz, H., Struck, U., Rossignol-Strick, M., Erlenkeuser, H., Howell, M. W., Kroon, D., Mackensen, A., Ishizuka, S., Oba, T., Sakamoto, T., Koizumi, I., 2003. Eastern Mediterranean surface water temperatures and $\delta^{18}O$ composition during deposition of sapropels in the late Quaternary. Paleoceanography 18, 1005. https://doi.org/10.1029/2000pa000617.
Farquhar, G.D., Ehleringer, J.R., Hubick, K.T., 1989. Carbon isotope discrimination and photosynthesis. Annual Review of Plant Physiology and Plant Molecular Biology 40, 503–537.
Farquhar, G.D., O'Leary, M.H., Berry, J.A., 1982. On the relationship between carbon isotope discrimination and the intercellular carbon dioxide concentration in leaves. Australian Journal of Plant Physiology 9, 121–137.
Foster, G.L., Royer, D.L., Lunt, D.J., 2017. Future climate forcing potentially without precedent in the last 420 million years. Nature Communications 8, 14845. https://doi.org/10.1038/ncomms14845.
Francois, R., Altabet, M.A., Goericke, R., McCorkle, D.C., Brunet, C., Poisson, A., 1993. Changes in the $\delta^{13}C$ of surface water particulate organic matter across the subtropical convergence in the SW Indian Ocean. Global Biogeochemical Cycles 7, 627–644.
Freeman, K.H., Hayes, J.M., 1992. Fractionation of carbon isotopes by phytoplankton and estimates of ancient CO_2 levels. Global Biogeochemical Cycles 6, 185–198.
Geerken, E., 2019. Elements in foraminiferal shells as recorders of past climates. Royal Netherlands Institude for Sea Research and Utrecht University 203, 111–125.
Giunta, S., Negri, A., Maffioli, P., Sangiorgi, F., Capotondi, L., Morigi, C., Principato, M. S., Corselli, C., 2006. Phytoplankton dynamics in the eastern Mediterranean Sea during Marine Isotopic Stage 5e. Palaeogeography, Palaeoclimatology, Palaeoecology 235, 28–47.
Goericke, R., Montoya, J.P., Fry, B., 1994. Physiology of isotopic fractionation in algae and cyanobacteria. In: Lajtha, K., Michener, R.H. (Eds.), Stable Isotopes in Ecology and Environmental Science. Blackwell, pp. 187–221.
Grant, K.M., Grimm, R., Mikolajewicz, U., Marino, G., Ziegler, M., Rohling, E.J., 2016. The timing of Mediterranean sapropel deposition relative to insolation, sea-level and African monsoon changes. Quaternary Science Reviews 140, 125–141.
Grelaud, M., Marino, G., Ziveri, P., Rohling, E.J., 2012. Abrupt shoaling of the nutricline in response to massive freshwater flooding at the onset of the last interglacial sapropel event. Paleoceanography 27, PA3208. https://doi.org/10.1029/2012PA002288.
Hayes, J.M., 1993. Factors controlling ^{13}C contents of sedimentary organic compounds: Principles and evidence. Marine Geology 113, 111–125.
Hayes, J.M., Freeman, K.H., Popp, B.N., Hoham, C.H., 1990. Compound-specific isotopic analyses: A novel tool for reconstruction of ancient biogeochemical processes. Organic Geochemistry 161, 103–125.
Hayes, J.M., Strauss, H., Kaufman, A.J., 1999. The abundance of ^{13}C in marine organic matter and isotopic fractionation in the global biogeochemical cycle of carbon during the past 800 Ma. Chemical Geology 16, 1115–1128.
Hollis, C.J., Dunkley Jones, T., Anagnostou, E., Bijl, P.K., Cramwinckel, M.J., Cui, Y., Dickens, G.R., Edgar, K.M., Eley, Y., Evans, D., Foster, G.L., Frieling, J., Inglis, G.N., Kennedy, E.M., Kozdon, R., Lauretano, V., Lear, C.H., Littler, K., Lourens, L., Nele Meckler, A., Naafs, B.D.A., Pälike, H., Pancost, R.D., Pearson, P.N., Röhl, U., Royer, D.L., Salzmann, U., Schubert, B.A., Seebeck, H., Sluijs, A., Speijer, R.P., Stassen, P., Tierney, J., Tripati, A., Wade, B., Westerhold, T., Witkowski, C., Zachos, J.C., Zhang, Y., Huber, M., Lunt, D.J., 2019. The DeepMIP contribution to PMIP4: Methodologies for selection, compilation and analysis of latest Paleocene and early Eocene climate proxy data, incorporating version 0.1 of the DeepMIP database. Geoscientific Model Development 12, 3149–3206.
Jasper, J.P., Hayes, J.M., 1990. A carbon isotope record of CO_2 levels during the late quaternary. Nature 347, 462–464.
Jasper, J.P., Hayes, J.M., Mix, A.C., Prahl, F.G., 1994. Photosynthetic fractionation of ^{13}C and concentrations of dissolved CO_2 in the central equatorial Pacific during the last 255,000 years. Paleoceanography 9, 781–798.
Kottmeier, D.M., Rokitta, S.D., Rost, B., 2016. Acidification, not carbonation, is the major regulator of carbon fluxes in the coccolithophore *Emiliania huxleyi*. New Phytologist 211, 126–137.
Küspert, W., 1982. Environmental changes during oil shale deposition as deduced from stable isotope ratios. In: Einsele, G., Seilacher, A. (Eds.), Cyclic and Event Stratification. Springer, Berlin, Heidelberg, pp. 482–501.
Laws, E.A., Bidigare, R.R., Popp, B.N., 1997. Effect of growth rate and CO_2 concentration on carbon isotopic fractionation by the marine diatom *Phaeodactylum tricornutum*. Limnology and Oceanography 42, 1552–1560.
Laws, E.A., Popp, B.N., Bidigare, R.R., Riebesell, U., Burkhardt, S., Wakeham, S.G., 2001. Controls on the molecular distribution and carbon isotopic composition of alkenones in certain haptophyte algae. Geochemistry, Geophysics, Geosystems 2, 1006. https://doi.org/10.1029/2000gc000057.
Lourens, L.J., Hilgen, F.J., Raffi, I., Vergnaud-Grazzini, C., 1996. Early Pleistocene chronology of the Vrica section (Calabria, Italy). Paleoceanography 11, 797–812.
Melki, T., Kallel, N., Fontugne, M., 2010. The nature of transitions from dry to wet condition during sapropel events in the Eastern Mediterranean Sea. Palaeogeography, Palaeoclimatology, Palaeoecology 291, 267–285.
Monnin, E., Indermühle, A., Dällenbach, A., Flückiger, J., Stauffer, B., Stocker, T.F., Raynaud, D., Barnola, J.M., 2001. Atmospheric CO_2 concentrations over the last glacial termination. Science 291, 112–114.
Mook, W.G., Bommerson, J.C., Staverman, W.H., 1974. Carbon isotope fractionation between dissolved bicarbonate and gaseous carbon dioxide. Earth and Planetary Science Letters 22, 169–176.
Müller, P.J., Kirst, G., Ruhland, G., Von Storch, I., Rosell-Melé, A., 1998. Calibration of the alkenone paleotemperature index $U^{K'}_{37}$ based on core-tops from the eastern South Atlantic and the global ocean (60°N–60°S). Geochimica et Cosmochimica Acta 62, 1757–1772.
Naafs, B.D.A., Castro, J.M., De Gea, G.A., Quijano, M.L., Schmidt, D.N., Pancost, R. D., 2016. Gradual and sustained carbon dioxide release during Aptian Oceanic Anoxic Event 1a. Nature Geoscience 9, 135. https://doi.org/10.1038/ngeo2627.
Oakes, J.M., Revill, A.T., Connolly, R.M., Blackburn, S.I., 2005. Measuring carbon isotope ratios of microphytobenthos using compound-specific stable isotope analysis of phytol. Limnology and Oceanography: Methods 3, 511–519.
Pagani, M., 2002. The alkenone-CO_2 proxy and ancient atmospheric carbon dioxide. Philosophical Transactions of the Royal Society A: Mathematical, Physical and Engineering Sciences 360, 609–632.
Pagani, M., 2013. Biomarker-based inferences of past climate: The alkenone pCO_2 proxy. In: Turekian, K., Heinrich, H. (Eds.), Treatise on Geochemistry: Second Edition, pp. 361–378.
Pagani, M., Arthur, M.A., Freeman, K.H., 1999. Miocene evolution of atmospheric carbon dioxide. Paleoceanography 14, 273–292.
Pagani, M., Zachos, J.C., Freeman, K.H., Tipple, B., Bohaty, S., 2005. Marked decline in atmospheric carbon dioxide concentrations during the Paleogene. Science 309, 600–603.
Pépin, L., Raynaud, D., Barnola, J.M., Loutre, M.F., 2001. Hemispheric roles of climate forcings during glacial-interglacial transitions as deduced from the Vostok record and LLN-2D model experiments. Journal of Geophysical Research Atmospheres 106, 31885–31892.
Petit, J.R., Jouzel, J., Raynaud, D., Barkov, N.I., Barnola, J.M., Basile, I., Bender, M., Chappellaz, J., Davis, M., Delaygue, G., Delmotte, M., Kotiyakov, V.M., Legrand, M., Lipenkov, V.Y., Lorius, C., Pépin, L., Ritz, C., Saltzman, E., Stievenard, M., 1999. Climate and atmospheric history of the past 420,000 years from the Vostok ice core, Antarctica. Nature 399, 429–436.
Popp, B.N., Laws, E.A., Bidigare, R.R., Dore, J.E., Hanson, K.L., Wakeham, S.G., 1998. Effect of phytoplankton cell geometry on carbon isotopic fractionation. Geochimica et Cosmochimica Acta 62, 69–77.
Popp, B.N., Takigiku, R., Hayes, J.M., Louda, J.W., Baker, E.W., 1989. The post-Paleozoic chronology and mechanism of ^{13}C depletion in primary marine organic matter. American Journal of Science 289, 436–454.
Rau, G.H., Riebesell, U., Wolf-Gladrow, D., 1996. A model of photosynthetic ^{13}C fractionation by marine phytoplankton based on diffusive molecular CO_2 uptake. Marine Ecology Progress Series 82, 269–279.
Raven, J.A., Beardall, J., 2014. CO_2 concentrating mechanisms and environmental change. Aquatic Botany 118, 24–37.
Reinfelder, J.R., 2011. Carbon concentrating mechanisms in eukaryotic marine phytoplankton. Annual Review of Marine Science 3, 291–315.
Riebesell, U., Zondervan, I., Rost, B., Tortell, P.D., Zeebe, R.E., Morel, F.M.M., 2000. Reduced calcification of marine plankton in response to increased atmospheric CO_2. Nature 407, 364–367.
Rivaro, P., Messa, R., Massolo, S., Frache, R., 2010. Distributions of carbonate properties along the water column in the Mediterranean Sea: Spatial and temporal variations. Marine Chemistry 121, 236–245.
Rohling, E.J., De Rijk, S., 1999. Holocene climate optimum and last glacial maximum in the Mediterranean: The marine oxygen isotope record. Marine Geology 153, 57–75.
Rost, B., Riebesell, U., Burkhardt, S., Sültemeyer, D., 2003. Carbon acquisition of bloom-forming marine phytoplankton. Limnology and Oceanography 48, 55–67.
Royer, D.L., 2013. Atmospheric CO_2 and O_2 during the Phanerozoic: Tools, patterns, and impacts. In: Turekian, K., Heinrich, H. (Eds.), Treatise on Geochemistry: Second Edition, pp. 251–267.
Sakata, S., Hayes, J.M., McTaggart, A.R., Evans, R.A., Leckrone, K.J., Togasaki, R.K., 1997. Carbon isotopic fractionation associated with lipid biosynthesis by a cyanobacterium: Relevance for interpretation of biomarker records. Geochimica et Cosmochimica Acta 61. 5379–5289.
Schouten, S., Klein Breteler, W.C.M., Blokker, P., Schogt, N., Rijpstra, W.I.C., Grice, K., Baas, M., Sinninghe Damsté, J.S., 1998. Biosynthetic effects on the stable carbon isotopic compositions of algal lipids: Implications for deciphering the carbon isotopic biomarker record. Geochimica et Cosmochimica Acta 62, 1397–1406.
Sinninghe Damsté, J.S., Kok, M.D., Köster, J., Schouten, S., 1998. Sulfurized carbohydrates: An important sedimentary sink for organic carbon? Earth and Planetary Science Letters 164. https://doi.org/10.1016/S0012-821X(98)00234-9.

Sinninghe Damsté, J.S., Kuypers, M.M.M., Pancost, R.D., Schouten, S., 2008. The carbon isotopic response of algae, (cyano)bacteria, archaea and higher plants to the late Cenomanian perturbation of the global carbon cycle: Insights from biomarkers in black shales from the Cape Verde Basin (DSDP Site 367). Organic Geochemistry 39, 1647–1816.

Stoll, H.M., Guitian, J., Hernandez-Almeida, I., Mejia, L.M., Phelps, S., Polissar, P., Rosenthal, Y., Zhang, H., Ziveri, P., 2019. Upregulation of phytoplankton carbon concentrating mechanisms during low CO_2 glacial periods and implications for the phytoplankton pCO_2 proxy. Quaternary Science Reviews 208, 1–20.

ten Haven, H.L., Baas, M., de Leeuw, J.W., Schenck, P.A., 1987a. Late Quaternary Mediterranean sapropels, I – On the origin of organic matter in sapropel S7. Marine Geology 75, 137–156.

ten Haven, H.L., Baas, M., de Leeuw, J.W., Schenck, P.A., Brinkhuis, H., 1987b. Late Quaternary Mediterranean sapropels II. Organic geochemistry and palynology of S1 sapropels and associated sediments. Chemical Geology 64, 149–167.

van Bentum, E.C., Reichart, G.J., Sinninghe Damsté, J.S., 2012. Organic matter provenance, palaeoproductivity and bottom water anoxia during the Cenomanian/Turonian oceanic anoxic event in the Newfoundland Basin (northern proto North Atlantic Ocean). Organic Geochemistry 50, 11–18.

van der Meer, M.T.J., Baas, M., Rijpstra, W.I.C., Marino, G., Rohling, E.J., Sinninghe Damsté, J.S., Schouten, S., 2007. Hydrogen isotopic compositions of long-chain alkenones record freshwater flooding of the Eastern Mediterranean at the onset of sapropel deposition. Earth and Planetary Science Letters 262, 594–600.

van Dongen, B.E., Schouten, S., Sinninghe Damsté, J.S., 2002. Carbon isotope variability in monosaccharides and lipids of aquatic algae and terrestrial plants. Marine Ecology Progress Series 232, 83–92.

Volkman, J.K., Eglinton, G., Corner, E.D.S., Forsberg, T.E.V., 1980. Long-chain alkenes and alkenones in the marine coccolithophorid *Emiliania huxleyi*. Phytochemistry 19, 2619–2622.

Weiss, R.F., 1974. Carbon dioxide in water and seawater: the solubility of a non-ideal gas. Marine Chemistry 2, 203–215.

Wilkes, E.B., Carter, S.J., Pearson, A., 2017. CO_2-dependent carbon isotope fractionation in the dinoflagellate *Alexandrium tamarense*. Geochimica et Cosmochimica Acta 212, 48–61.

Wilkes, E.B., Pearson, A., 2019. A general model for carbon isotopes in red-lineage phytoplankton: Interplay between unidirectional processes and fractionation by RubisCO. Geochimica et Cosmochimica Acta 265, 163–181.

Witkowski, C.R., Agostini, S., Harvey, B.P., van der Meer, M.T.J., Sinninghe Damsté, J. S., Schouten, S., 2019. Validation of carbon isotope fractionation in algal lipids as a pCO_2 proxy using a natural CO_2 seep (Shikine Island, Japan). Biogeosciences 16, 4451–4461.

Witkowski, C.R., van der Meer, M.T.J., Smit, N.T., Sinninghe Damsté, J.S., Schouten, S., 2020. Testing algal-based pCO_2 proxies at a modern CO_2 seep (Vulcano, Italy). Scientific Reports 10, 10508. https://doi.org/10.1038/s41598-020-67483-8.

Witkowski, C.R., Weijers, J.W.H., Blais, B., Schouten, S., Sinninghe Damsté, J.S., 2018. Molecular fossils from phytoplankton reveal secular pCO_2 trend over the phanerozoic. Science Advances 4, eaat4556. https://doi.org/10.1126/sciadv.aat4556.

Zhang, Y.G., Henderiks, J., Liu, X., 2020. Refining the alkenone-pCO_2 method II: Towards resolving the physiological parameter 'b'. Geochimica et Cosmochimica Acta 281, 118–134.

Zhang, Y.G., Pagani, M., Liu, Z., Bohaty, S.M., Deconto, R., 2013. A 40-million-year history of atmospheric CO_2. Philosophical Transactions of the Royal Society A: Mathematical, Physical and Engineering Sciences 371, 20130096. https://doi.org/10.1098/rsta.2013.0096.

Zhang, Y.G., Pearson, A., Benthien, A., Dong, L., Huybers, P., Liu, X., Pagani, M., 2019. Refining the alkenone-pCO_2 method I: Lessons from the quaternary glacial cycles. Geochimica et Cosmochimica Acta 260, 177–191.